How to cite: *Angew. Chem. Int. Ed.* **2022,** *61,* e202212245
International Edition: doi.org/10.1002/anie.202212245
German Edition: doi.org/10.1002/ange.202212245

Surface Chemistry

Surface Diffusion Aided by a Chirality Change of Self-Assembled Oligomers under 2D Confinement

Abhijit Bera, Stefan Henkel, Joel Mieres-Perez, Yetsedaw Andargie Tsegaw, Elsa Sanchez-Garcia, Wolfram Sander, and Karina Morgenstern**

Abstract: Chirality switching of self-assembled molecular structures is of potential interest for designing functional materials but is restricted by the strong interaction between the embedded molecules. Here, we report on an unusual approach based on reversible chirality changes of self-assembled oligomers using variable-temperature scanning tunneling microscopy supported by quantum mechanical calculations. Six functionalized diazomethanes each self-assemble into chiral wheel-shaped oligomers on Ag(111). At 130 K, a temperature far lower than expected, the oligomers change their chirality even though the molecules reside in an embedded self-assembled structure. Each chirality change is accompanied by a slight center-of-mass shift. We show how the identical activation energies of the two processes result from the interplay of the chirality change with surface diffusion, findings that open the possibility of implementing various functional materials from self-assembled supramolecular structures.

Introduction

Over the past decade, the field of surface modification by self-organized molecular systems has received immense scientific attention. The main thrust is to define novel materials and identify their exciting properties. In general, self-assembly is controlled by specific functionalized groups that lead to van-der-Waals[1] or Coulomb interactions[2] or hydrogen[3] or halogen bonding.[4] During self-assembly, the molecules diffuse and adjust their orientation to form a specific structure on the surface.[5] The general principles of self-assembled structures have proven to be particularly interesting for understanding aspects of the chiral phenomena of organic molecules on solid surfaces.[6] The non-centrosymmetric nature of an interface ensures that chirality is achieved in two dimensions (2D) even by prochiral molecules on achiral surfaces because of symmetry loss in the adsorbed state.[6a,7] Such 2D chirality has attracted considerable interest in areas as diverse as molecular recognition,[8] heterogeneous catalysis,[9] and sensing technology.[10] STM studies of self-assembled molecular layers adsorbed in a crystalline substrate reveal several chiral structures, such as the formation of homochiral domains,[11] racemic clusters,[12] or handed nanostructures.[13]

The active control of the chirality on surfaces has been achieved so far above a critical coverage[5a,7a] or by the sergeant-soldiers method.[14] Moreover, the chirality was switched by an external electric field, hot electrons, or light for both single molecules and layers of self-assembled monolayers.[15] Recently, local chiral inversion was induced by manipulating other small molecules involved in the nanostructure formation.[16] An exception to chirality control is a thermally-induced chirality switching through the conformational changes of one side group.[7b] The reason is that other dynamic processes, such as molecular diffusion or rotation, may concurrently occur in a molecular system, and each of these processes needs to be appropriately addressed to understand the chirality change. Understanding the chirality change in conjunction with the diffusion of chiral assemblies might thus be essential for several catalytic reactions and storage applications but has not yet been discussed.

The most important of these processes is surface diffusion. It controls surface reactions by allowing the reactants to reach specific reactive sites. The surface diffusion of small inorganic molecules like CO and H_2O is well understood and can essentially be described as a simple hopping motion.[17] Increased complexity results from dimer and trimer formation.[17a,18] Studies for larger organic molecules are rare and point to increased complexity.[19] For instance, the motion of 4-trans-2-(pyrid-4-yl-vinyl)benzoic acid (PVBA) on the anisotropic Pd(110) is restricted to one dimension.[19a] For cobalt phthalocyanine molecules on Ag-(100), rotational and translation movements are associated with activation energies of the same order.[19d] Studies for clusters of molecules are even rarer and so far restricted to

[*] Prof. Dr. A. Bera, Prof. Dr. K. Morgenstern
Physikalische Chemie I, Ruhr-Universität Bochum
Universitätsstr. 150, 44801 Bochum (Germany)
E-mail: abhijit.bera@midnaporecollege.ac.in
karina.morgenstern@rub.de

Dr. S. Henkel, Dr. Y. Andargie Tsegaw, Prof. Dr. W. Sander
Organic Chemistry II, Ruhr-Universität Bochum
Universitätsstr. 150, 44801 Bochum (Germany)

Dr. J. Mieres-Perez, Prof. Dr. E. Sanchez-Garcia
Computational Biochemistry, Universität Duisburg-Essen
Universitätsstr. 2, 45141 Essen (Germany)

dimers.[20] These studies suggest an even richer complexity for the diffusion of self-assembled oligomers.

In this article, we report on the formation of chiral self-assembled oligomers from functionalized diazomethane. Six molecules of *p*-tolyl(trifluoromethyl)diazomethane (PTTDM) form oligomers on Ag(111). The kinetics of these oligomers, both their chirality changes and diffusion, are investigated by time-lapsed STM and quantum mechanical calculations. Temperature-dependent measurements yield the activation energies involved in the chirality change and diffusion. The possible kinetic pathways are discussed, and a design strategy is proposed for a supramolecular structure allowing a chirality change at room temperature.

Results and Discussion

p-tolyl(trifluoromethyl)diazomethane (PTTDM) (Figure 1a) was used for this study because of (a) its specific charge distribution (Figure 1b) and (b) its 2D chirality on the surface (Figure 1c). Prominent electrophilic and nucleophilic centers on the electrostatic potential (ESP) map are the central nitrogen atom of the diazo ($-N_2$) group and the fluorine atoms of the $-CF_3$ group, respectively. These regions are expected to dominate structure formation under two-dimensional confinement conditions, while the largely charge-neutral methyl group should hinder an agglomeration of larger clusters. Under two-dimensional confinement, the two groups attached to the benzylic carbon atom, i.e., the $-CF_3$ and $-N_2$ groups, lead to two mirror-symmetric enantiomers, named L- and R-type (Figure 1c).[21]

At low coverage, the elongated and slightly curved protrusions agglomerate at the step edges without any preferred orientation (Figure 2a,b). The size and elongated shape of the molecule (0.85 ± 0.10) nm match well with the size and shape of the computed structure (0.86 nm), suggesting the planar adsorption of the molecule. While their size and elongated shape fit the molecular dimension, the banana shape is surprising at first sight. For a related molecule, diazoflourene on Ag(111), the diazo group was invisible to STM.[5e] On the other hand, methyl groups always appear as round features in STM images.[22] Thus, the

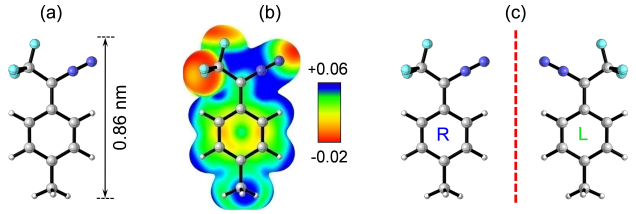

Figure 1. Properties of PTTDM. a) Optimized geometry of PTTDM at the B3LYP-D3/def2-TZVP level of theory (light blue, blue, grey, white; F, N, C, H). b) Electrostatic potential map (ESP, at the same level of theory) projected on a contour value of 7×10^{-6} e nm^{-3}, the electron density is given in fractions of the elementary charge with red corresponding to −0.02 Hartree, and blue to 0.06 Hartree. c) Two surface enantiomers, R- and L-type, the dashed line indicates the mirror plane.

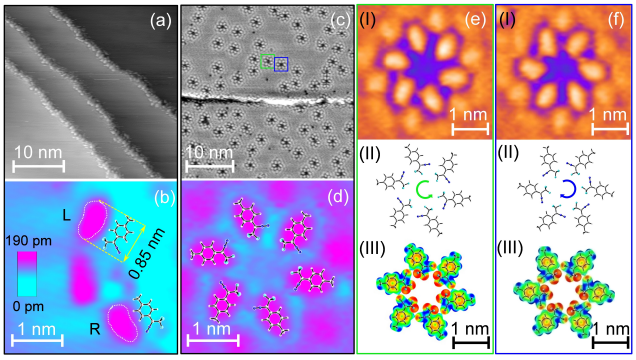

Figure 2. Adsorption of PTTDM molecules on Ag(111). a,c) large scale, b,d) small-scale, and e,f) high-resolution STM images for a coverage of a,b) 0.2 ML and c–f) 0.4 ML. Light blue and bright pink in (b, d) represent the Ag(111) surface and the PTTDM molecules, respectively. White dotted lines follow the contour of the molecules. Ball-and-stick models of calculated structures are placed next to (b) or superimposed to (d) some of the molecules. e,f) High-resolution STM images (I) focusing on the two oligomers marked by squares in panel (c), with the corresponding optimized geometries under symmetry constraints (II) and ESP maps (III). Blue and green arrows indicate clockwise and counterclockwise orientations of the oligomers. Scanning conditions: $V = 120$ mV, $I = 60$ pA, $T = (122 \pm 2)$ K.

banana shape of the molecules is attributed to the specific positions of the methyl and the $-CF_3$ group with respect to the molecular axis. From the asymmetric shape, we determine the surface-induced chirality of the molecules, marked by L and R in Figure 2b, which exist in equal amounts on the surface (50 molecules analyzed). The agglomeration of the molecules at the step edges implies that the molecules are mobile enough to diffuse to the step edges at the deposition temperature of (115 ± 5) K.

Having identified individual molecules, we now turn to the formation of self-assembled oligomers formed at the same temperature at a slightly higher coverage of 0.4 ML (Figure 2c). At this coverage, both sides of the step edges are entirely decorated by molecules (Figure 2c, middle). Additionally, there are circular structures distributed randomly across the terraces. The terrace between these circular structures appears brighter than at lower coverage (Figure 2a). It is also imaged brighter than the interior of the circular structures. Such a diffusive background points to highly mobile molecules crossing multiple times under the tip during the scanning.[22] The formation of the self-assembled oligomers is possible in the coverage range of 0.3 ML to 0.6 ML (see Supporting Information, Section 3.1).

The circular structures are monodispersed wheel-shaped oligomers consisting of six molecules (Figure 2d). The direct comparison of neighboring oligomers reveals two types of these self-assembled oligomers (Figure 2c, Figure S2). The two wheels appear inclined in opposite directions, better visible in a close-up view (Figure 2e,f). The close-up view reveals that the diffusive noise around the oligomers is structured, reflecting transient bindings of molecules from the diffusive background. The structured pattern is discussed in the Supporting Information, Section 3.2. The shape of the oligomers is not altered, suggesting a weaker interaction of

the mobile molecules with the oligomers. From the orientations of the banana-shaped protrusions, we infer that the two opposite pinwheel configurations are enantiopure. Their formation may result from the interaction of the charged groups.

We analyze the intermolecular interactions that stabilize the oligomers based on high-resolution STM images with optimization of an assembly of six molecules at the B3LYP-D3/def2-TZVP level of theory. In the gas phase calculations, the 2D confinement by the surface is not present, and the optimized oligomer would not be planar. Therefore, the geometry was restricted to the C_{6h} point group. The calculated geometry (Figure 2e,f, II) and the ESP maps of the two mirror images (Figure 2e,f, III of the oligomers) match well with the acquired STM images (Figure 2e,f, I). However, the resulting C_{6h} symmetric structure features imaginary frequencies between 10 and 15 cm^{-1}, corresponding to a lowering in symmetry. Thus, the chiral self-assembled oligomers are formed by a combination of intermolecular interactions and surface interactions; both are essential.

For more insight into the formation and stability of the oligomers, we performed gas-phase quantum mechanics (QM) molecular dynamics simulations at temperatures from 50 K to 128 K in 10 K intervals. For details, see Supporting Information, section 4.1. The molecular dynamic simulations suggest that the intermolecular interactions in the gas-phase are insufficient to stabilize the oligomers.

We performed DFT calculations of PTTDM on Ag (111) using dimers of PTTDM as models to study the interactions present in the oligomer and the interactions between its components and the surface at a reasonable computational cost. We found several nearly isoenergetic adsorbed dimers on the surface that differ in the adsorption sites for the different chemical groups of the molecules (Supporting Information, Figure S4). The largest energy difference among them is 2 kcal mol^{-1}. For all of them, the calculations predict a close to planar adsorption on the surface (Figure 3 and Figure S4). The diazo groups are tilted, with the terminal N atom closest to the surface atoms. In the adsorbed dimers, the N1···H distances range from 0.262 nm to 0.273 nm, and the C1–H1···N1 angles are close to 160° (Table S1). Within this distance range, electrostatic interactions between the $–CF_3$ and $–N_2$ groups should contribute to the overall stability of the dimer and consequently the oligomer (Figure 2e,f), because of the proximity of the $–N_2$ of one molecule and the F atom (closest to the surface) of the $–CF_3$ group of an adjacent molecule, ranging from 0.299 nm to 0.369 nm (Table S1 and Figure S4). On the other hand, the overall calculated adsorption energies ranged from 40 to 42 kcal mol^{-1} for all dimers. These values represent the adsorption energies with respect to the dimer (calculated in the gas-phase) and the pristine surface, defined such that the larger the positive values, the more stable the adsorbed dimer with respect to the separated fragments. For two individual PTTDM molecules in the gas-phase (not forming a dimer) the adsorption energy is 44 to 45 kcal mol^{-1}, even larger than the dimer adsorption energy as a consequence of the enhanced stability of the gas-phase dimer with respect to the monomer. Both scenarios point to weak adsorption of PTTDM dimers, in agreement with the experimentally observed mobility of the oligomers on the surface. These results suggest that the combination of the weak intermolecular interactions between the molecules forming the complex and, more importantly, the interaction of those molecules with the surface, stabilize the experimentally observed oligomer. In addition, the existence of several nearly isoenergetic dimers facilitates a diffusive motion of the oligomers across the surface.

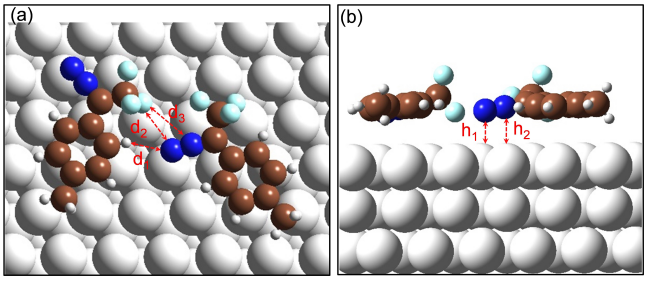

Figure 3. Adsorption structure of a PTTDM dimer on Ag (111). a) Top view with relevant intermolecular interactions, the atomic distances, d_1: N1-H, d_2: N1-F, and d_3: N2-F are marked. b) Side view marking the distance with respect to the Ag surface atoms, h_1: N1-Ag, and h_2: N2-Ag. For the other dimers, see Supporting Information, Figure S4.

Based on the calculated adsorption structure of the PTTDM dimer and their calculated STM image (see Supporting Information, Figure S6) in conjunction with the STM images of the oligomer, we derive model structures of the oligomers on Ag(111). Their azimuthal orientations differ by $(16\pm2)°$, and the individual molecules and their corresponding oligomers axes are inclined by $\gamma=(8\pm1)°$ to the left or the right sides of the Ag(111) close-packed lattice directions (compare Figure 4b,c). For the detailed geometrical analysis of the oligomers on Ag(111), see Supporting Information, section 5.1. Based on the dimer calculations, three adsorption sites of the Ag(111) are equally likely for these oligomers. Their center might be above an atop site, an hcp site, or an fcc site. In We present in Figures 4f and 4g the model for the atop site. For the other models, see Supporting Information, section 5.2.

Independently from this assignment, the tolyl cores of all six molecules are almost aligned with the closed-packed lattice directions. For the center of the oligomer above an atop site, the positively and negatively charged nitrogen atoms of the diazo group are situated close to an electron-rich three-fold hollow site and an electron-deficient atop site, respectively, a binding that is consistent with calculations of the PTTDM dimer on the surface (Figure 3). Due to the threefold symmetry of the surface, the tolyl groups and the positively charged N atoms of the diazo group of the adjacent molecules are located alternately nearby hcp or fcc sites, as demonstrated by a close-up view of two neighboring L-type molecules in Figure 4h. The correlation between the chirality of the oligomers and that of the partaking surface enantiomers most likely results from the interactions between the polar groups.

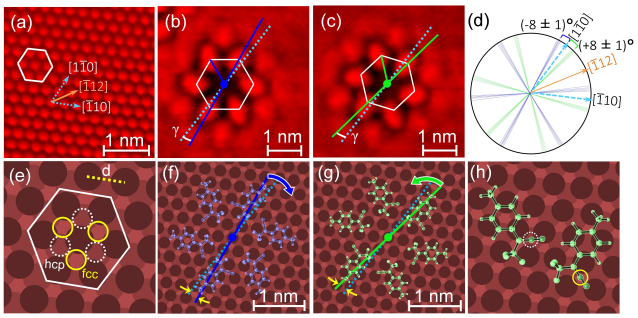

Figure 4. Adsorption models of self-assembled oligomers on Ag(111). a) Atomic resolution STM image of Ag(111); a hexagon comprising seven atoms for comparison with the six-fold symmetry of oligomers; arrows indicate surface directions. b,c) STM images of R- and L-type self-assembled oligomers. d) Angular plot of the direction of R- (blue) and L-type (green) molecules on Ag(111) with respect to the surface directions. e) Ball model of the three top layers of Ag(111). Dark, faded, and light brown balls represent the topmost, second, and third surface layer atoms. Fcc and hcp sites marked by yellow and white circles, respectively. f,g) Ball-and-stick models of R- and L-type oligomers on Ag(111) surface. Cyan lines indicate one of the close-packed <110> surface directions. Blue and green lines designate R- and L-type oligomer axes. Blue and green arrows denote the clockwise and counterclockwise orientation of the two oligomers with respect to the <110> surface directions. h) Enlarged view of the surface adsorption sites of two adjacent molecules in an L-type oligomer. Scanning conditions a) $V=70$ mV, $I=200$ pA, T: RT and b,c) $V=120$ mV, $I=60$ pA, $T=(122\pm2)$ K.

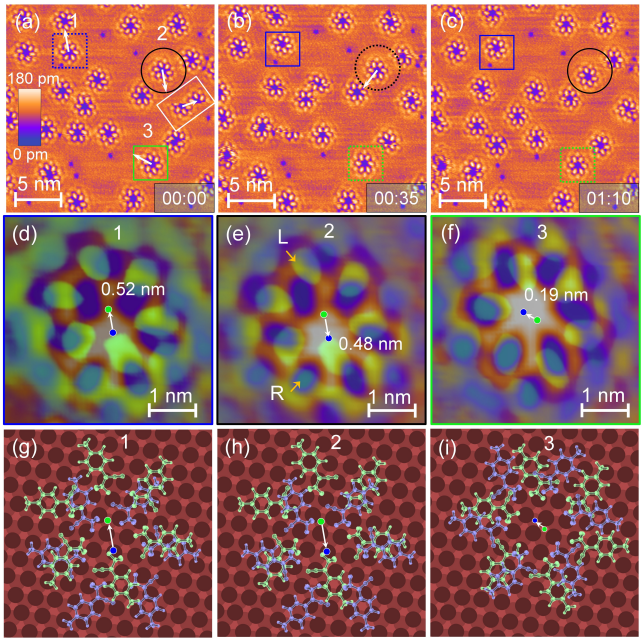

Figure 5. Reversible chirality change of self-assembled oligomers. a–c) Three consecutive STM images recorded at the same spot of the surface at a scanning speed of 35 s frame^{-1}. Open circles and square boxes mark R-type oligomers, and filled circles and boxes mark L-type oligomers. The positions of circles and boxes are at the same positions in all panels. Arrows indicate the directions of the displacements. The white rectangular box represents a mobile structure imaged during its motion. The blue boxes mark a chirality change from R- to L-type (b), which persists in the next frame (c). Black circles mark a reversible change, i.e., L- to R- (b) and R- to L-type (c). The green box marks an L- to R-type change (b), which remains in R-type chirality (c). d–f) Superposition of two successive STM images and g–i) corresponding ball-stick model of the oligomers (blue: R-type and green: L-type) marked 1, 2, and 3 in panel (a). Arrow indicates center-of-mass movement from the initial to the final position. Scanning conditions: $V=120$ mV, $I=60$ pA, $T=(126\pm1)$ K.

Having understood the structure formation and the adsorption geometry of the chiral self-assembled oligomers of PTTDM, we now turn to the thermal switching of their chirality. Time-lapse sequences of STM images, so-called movies, reveal a center-of-mass (CM) motion of the oligomers, some of them accompanied by a change of the chirality (Figure 5a to 5c, see Supporting Information for an STM movie). The chirality changes from R- to L-type (blue box) and from L- to R-type (green box) may happen at a temperature as low as 122 K within as little time as 35 s. The chirality change is reversible (black circle). Note that a chirality change is always accompanied by a CM motion, as demonstrated by the superposition of two successive STM images (Figure 5d–f) and the corresponding ball-stick models (Figure 5g–i). In contrast, CM motions without a chirality change are frequently observed. In fact, it is expected that only half of the observed motions, i.e., those with an odd number of chirality changes, display a visible chirality change, but those with an even number do not. Furthermore, the diffusion is fast on the timescale of the measurement as within one line (i.e., 90 ms), an oligomer is imaged at two different positions, as shown in Figure 5a (white rectangular box). The accessible temperature range for reliable statistics was from 122 K to 132 K for both the chirality change and the diffusion.

Before determining the two activation energies, we discuss the details of the motion and chirality change of an individual oligomer. The oligomer marked in Figure 6a diffuses at 124 K to 128 K with respect to some immobile depressions by randomly jumping between discrete positions. During that diffusion, it occasionally changes its chirality. For the track of another oligomer for 20 min at the same temperature, the two enantiomers are marked by blue and green points and superimposed to an atomically resolved Ag(111) image (Figure 6b). The oligomer frequently changes its chirality during its diffusion between different adsorption sites, including the hollow sites of Ag(111). The minimum distance traversed by an oligomer accompanied by a change of its chirality is (0.20 ± 0.05) nm, in agreement with the distance between an fcc and an hcp site, smaller than a lattice constant. Greater distances reflect multiple chirality changes between the images. From such observations, we conclude that the oligomer prefers to adopt a different adsorption site upon changing its chirality. Note that the transiently bound peripheral molecules might alter the diffusivity of oligomers quantitatively, but the influence is expected to be low due to the transient nature of binding.

To determine the activation energy for diffusion, we follow the center-of-mass motion of individual oligomers over extended periods, disregarding their chirality change. We performed a statistical analysis of the oligomer diffusion

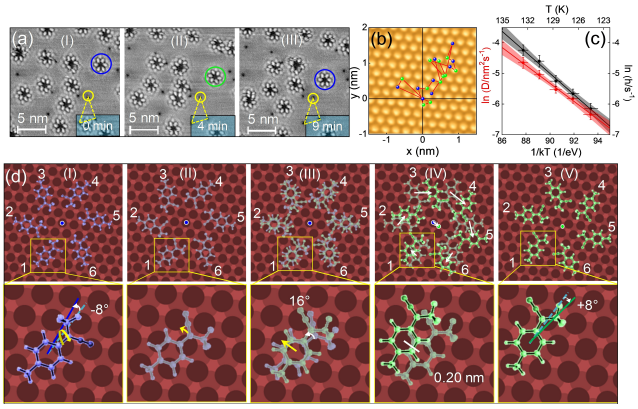

Figure 6. Surface diffusion aided by a chirality change of self-assembled oligomers on Ag(111). a) Series of STM images at indicated times. Yellow dashed triangles mark three immobile depressions (one of them in yellow circles) used as a reference for the motion. Scanning conditions: $V=120$ mV, $I=60$ pA, $T=(124$ to $128)$ K. b) Track of the center-of-mass positions of one oligomer with the color of the circles reflecting its chirality (blue: R-type) and (green: L-type). c) Arrhenius plot of two-dimensional diffusivity (D, red, left axis) and rate of chirality change (h, black, right axis) of the oligomers versus inverse temperature with fits. Horizontal bars mark the range of temperature contributing to the data point. Vertical error bars represent the standard deviation. d) Schematics of chirality change and surface diffusion of oligomers. Initial adsorption structure (R-type) (I), chirality change of individual molecules (II), 16° rotation of the whole molecules (III), diffusion of each molecule (IV), and final adsorption structure (L-type) (V). Blue and green lines and dots correspond to the R- and L-type molecular axis and the center-of-mass of the oligomers, respectively.

at different temperatures from time-lapsed STM images.[19d] The Arrhenius plot of the two-dimensional diffusivity (D) in Figure 6c (red) yields the activation energy for diffusion $E_d=(0.30\pm0.05)$ eV with a prefactor of $D_0=2.1\times10^{9\pm1.4}$ nm^{2}s^{-1}. Adapting a commonly used model to study the diffusion of molecules on surfaces,[24] the activation energy for the chirality changes is determined to be $E_a=(0.34\pm0.07)$ eV with a prefactor of $h_0=9.24\times10^{10\pm1.8}$ s^{-1}. The low prefactors indicate processes that consist of several consecutive steps. The calculated rotational barrier of one trifluoromethyl diazomethane (TDM) group within a PTTDM molecule on Ag(111) is, at 0.43 eV (Supporting Information, Figure S9), considerably larger than the gas-phase barrier, at 0.13 eV, and slightly higher than the experimentally determined range of (0.34 ± 0.7) eV for the chirality change of the oligomer. Details of the dynamical processes are discussed in Supporting Information, Section 6.

The separately determined energy barriers for chirality change and diffusion are the same within the error margin. Thereby, the activation energy for the chirality change of the oligomers is in the same range as previously determined activation energies for chirality changes of large organic molecules. For instance, a chirality switching through conformational changes by cis-trans and trans-cis flipping of the end groups of 1,4-bis[(5-tert-butyl-3-formyl-4-hydroxyphenyl)ethynyl]benzene on Au(111) has an activation energy of (0.30 ± 0.02) eV.[7b] Or, a caged trimeric supramolecular unit of a rod-like para-sexiphenyl-dicarbonitrile (NC-Ph$_6$-CN) molecule switched its chirality with an activation energy of (0.26 ± 0.01) eV.[25] In contrast, the activation energies for the diffusion of some large organic molecules, e.g., PVBA (0.83 eV),[19a] DC (0.71 eV),[24] and HtBDC (0.57 eV),[24] are typically much larger than the oligomers diffusion energy barrier of (0.30 ± 0.05) eV, determined here. Only in one case, for cobalt phthalocyanine (CoPc) on Ag(100), the diffusion energy barrier of (0.16 ± 0.01) eV[19d] is considerably smaller than the oligomer diffusion barrier. In this case, the low diffusion barrier was facilitated by a rotational motion. These comparisons suggest that here the chirality change enables the low diffusion barrier.

The most likely scenario of the chirality change is initiated by a rotation of one of the trifluoromethyl diazomethane (TDM) groups (Figure 1c), leading to a chirality change of one of the molecules (Figure 6d, I). All other molecules need to follow this chirality change retaining favorable bonding, leading to unfavorable orientations for the intermolecular bonds (II in Figure 6d). Thus, each molecule needs to rotate by 16° to restore a favorable orientation, leaving the molecules in unfavorable adsorption sites (III). With the initial molecule moving to its closest favorable adsorption site, the other molecules need to move by different distances (IV). Overall, the center-of-mass of the oligomer shifts to a different adsorption site (here from a hollow to atop site) (V), a distance corresponding to the smallest displacement observed in the experiment. This process allows a chirality change of the wheel without its disintegration, i.e., the molecules remain bound in their original wheel. We infer that the chirality change of the oligomer, initiated by a chirality change of a single molecule, is intimately connected to its CM motion.

Conclusion

Our combined time-lapsed STM and computational studies revealed how the two enantiomers of PTTDM (p-tolyl(trifluoromethyl)diazomethane) self-assemble into two enantiomeric-pure chiral wheel-shaped oligomers on Ag(111) based on weak non-covalent interactions. The interactions between the molecules in the self-assembled oligomers are too weak to stabilize them in the gas phase. But it is stable on the surface due to its 2D confinement effect. The interconversion between two chiral oligomers is aided by a facile chirality change of individual molecules, causing a small center-of-mass motion of the oligomers and promoting large-scale diffusion. It occurs even though the molecules reside in an embedded self-assembled structure. Therefore, the chirality changes of the oligomers with an activation energy of (0.34 ± 0.07) eV ease their diffusion at a much lower temperature than other large molecules. Our investigations demonstrate the dynamical phenomena of the supramolecular species by utilizing a weak intermolecular interaction concept of self-assembled oligomers. These dynamics are crucial to synthesizing complex structures on

surfaces, in which functional molecular systems control a chemical reaction by directing its enantioselectivity.

While we analyzed PTTDM only in the temperature range between 120 and 132 K, we identified three main principles that need to be fulfilled for the chirality-change-induced surface diffusion of oligomers: (i) The nucleophilic and electrophilic parts of the molecule should be in close proximity to form an inner ring protected by neutral end groups. (ii) The chirality change of the molecule needs to be facile, here facilitated by the single bond between the phenyl carbon and the side group carbon. (iii) The intermolecular binding energy must be higher than the energy barrier of this chirality change. By tuning the latter point, another temperature range should be reachable, possibly also room temperature.

We anticipate that this work will motivate further research on the detailed mechanisms of the chirality-change-induced surface diffusion to fabricate an efficient molecular system in due course. For instance, with higher intramolecular interaction energy, the energy needed for the chirality change could be higher, such that the phenomenon should be observable at a higher temperature.

Experimental Section

Detailed information on materials, methods, and computations is available in the Supporting Information.

Acknowledgements

The authors thank Prof. Dr. Grazyna Antczak, Wroclaw University, Poland, for the fruitful discussion concerning the diffusivity analysis. This work was supported by the Research Training Group "Confinement-controlled Chemistry," which is funded by the Deutsche Forschungsgemeinschaft (DFG; Grant No. GRK2376/331085229). This work was also funded by the Deutsche Forschungsgemeinschaft (DFG; German Research Foundation) under Germany's Excellence Strategy-Grant No. EXC 2033-390677874-RESOLV. The computational work was funded by the Deutsche Forschungsgemeinschaft (DFG; Grant No. 436586093). Open Access funding enabled and organized by Projekt DEAL.

Conflict of Interest

The authors declare no conflict of interest.

Data Availability Statement

The data that support the findings of this study are available in the supplementary material of this article.

Keywords: 2D Confinement Structure · Chirality Change · Diazomethane · Self-Assembled Oligomer · Surface Diffusion

[1] T. Yokoyama, S. Yokoyama, T. Kamikado, Y. Okuno, S. Mashiko, *Nature* **2001**, *413*, 619–621.
[2] L. Xie, Y. Ding, X. Wang, W. Xu, *Phys. Chem. Chem. Phys.* **2019**, *21*, 9357–9361.
[3] a) J. V. Barth, J. Weckesser, C. Cai, P. Günter, L. Bürgi, O. Jeandupeux, K. Kern, *Angew. Chem. Int. Ed.* **2000**, *39*, 1230–1234; *Angew. Chem.* **2000**, *112*, 1285–1288; b) A. G. Slater, L. M. A. Perdigão, P. H. Beton, N. R. Champness, *Acc. Chem. Res.* **2014**, *47*, 3417–3427.
[4] a) J. Lawrence, G. C. Sosso, L. Đorđević, H. Pinfold, D. Bonifazi, G. Costantini, *Nat. Commun.* **2020**, *11*, 2013; b) C. Bertram, D. Miller, C. Schunke, I. Kemeny, M. W. Kimura, U. Bovensiepen, E. Zurek, K. Morgenstern, *J. Phys. Chem. C* **2022**, *126*, 588–596.
[5] a) M. O. Lorenzo, V. Humblot, P. Murray, C. J. Baddeley, S. Haq, R. Raval, *J. Catal.* **2002**, *205*, 123–134; b) N. Wintjes, D. Bonifazi, F. Cheng, A. Kiebele, M. Stöhr, T. Jung, H. Spillmann, F. Diederich, *Angew. Chem. Int. Ed.* **2007**, *46*, 4089–4092; *Angew. Chem.* **2007**, *119*, 4167–4170; c) D. Heim, K. Seufert, W. Auwärter, C. Aurisicchio, C. Fabbro, D. Bonifazi, J. V. Barth, *Nano Lett.* **2010**, *10*, 122–128; d) K. S. Mali, D. Wu, X. Feng, K. Müllen, M. Van der Auweraer, S. De Feyter, *J. Am. Chem. Soc.* **2011**, *133*, 5686–5688; e) K. Lucht, I. Trosien, W. Sander, K. Morgenstern, *Angew. Chem. Int. Ed.* **2018**, *57*, 16334–16338; *Angew. Chem.* **2018**, *130*, 16572–16576.
[6] a) R. Cortés, A. Mascaraque, P. Schmidt-Weber, H. Dil, T. U. Kampen, K. Horn, *Nano Lett.* **2008**, *8*, 4162–4167; b) J. A. A. W. Elemans, I. De Cat, H. Xu, S. De Feyter, *Chem. Soc. Rev.* **2009**, *38*, 722–736.
[7] a) F. Vidal, E. Delvigne, S. Stepanow, N. Lin, J. V. Barth, K. Kern, *J. Am. Chem. Soc.* **2005**, *127*, 10101–10106; b) S. Weigelt, C. Busse, L. Petersen, E. Rauls, B. Hammer, K. V. Gothelf, F. Besenbacher, T. R. Linderoth, *Nat. Mater.* **2006**, *5*, 112–117.
[8] H. Cun, Y. Wang, B. Yang, L. Zhang, S. Du, Y. Wang, K.-H. Ernst, H.-J. Gao, *Langmuir* **2010**, *26*, 3402–3406.
[9] a) H.-U. Blaser, *Tetrahedron: Asymmetry* **1991**, *2*, 843–866; b) M. O. Lorenzo, S. Haq, T. Bertrams, P. Murray, R. Raval, C. J. Baddeley, *J. Phys. Chem. B* **1999**, *103*, 10661–10669; c) G. J. Hutchings, *Annu. Rev. Mater. Res.* **2005**, *35*, 143–166.
[10] W. Zou, Y. Yan, J. Fang, Y. Yang, J. Liang, K. Deng, J. Yao, J. Wei, *J. Am. Chem. Soc.* **2014**, *136*, 578–581.
[11] H. Chen, L. Tao, D. Wang, Z.-Y. Wu, J.-L. Zhang, S. Gao, W. Xiao, S. Du, K.-H. Ernst, H.-J. Gao, *Angew. Chem. Int. Ed.* **2020**, *59*, 17413–17416; *Angew. Chem.* **2020**, *132*, 17566–17569.
[12] J. Seibel, M. Parschau, K.-H. Ernst, *J. Am. Chem. Soc.* **2015**, *137*, 7970–7973.
[13] K. Tahara, A. Noguchi, R. Nakayama, E. Ghijsens, S. De Feyter, Y. Tobe, *Angew. Chem. Int. Ed.* **2019**, *58*, 7733–7738; *Angew. Chem.* **2019**, *131*, 7815–7820.
[14] a) A. Nuermaimaiti, C. Bombis, M. M. Knudsen, J. R. Cramer, E. Lægsgaard, F. Besenbacher, K. V. Gothelf, T. R. Linderoth, *ACS Nano* **2014**, *8*, 8074–8081; b) Y. Fang, E. Ghijsens, O. Ivasenko, H. Cao, A. Noguchi, K. S. Mali, K. Tahara, Y. Tobe, S. De Feyter, *Nat. Chem.* **2016**, *8*, 711–717.
[15] a) P. Mishra, J. P. Hill, S. Vijayaraghavan, W. Van Rossom, S. Yoshizawa, M. Grisolia, J. Echeverria, T. Ono, K. Ariga, T. Nakayama, C. Joachim, T. Uchihashi, *Nano Lett.* **2015**, *15*, 4793–4798; b) J. A. Elemans, *Adv. Funct. Mater.* **2016**, *26*, 8932–8951; c) Y. L. Wang, K. Sun, Y. B. Tu, M. L. Tao, Z. B. Xie, H. K. Yuan, Z. H. Xiong, J. Z. Wang, *Phys. Chem. Chem. Phys.* **2018**, *20*, 7125–7131.
[16] a) D. Li, L. Sun, Y. Ding, M. Liu, L. Xie, Y. Liu, L. Shang, Y. Wu, H.-J. Jiang, L. Chi, X. Qiu, W. Xu, *ACS Nano* **2021**, *15*,

16896–16903; b) L. Xie, Y. Ding, D. Li, C. Zhang, Y. Wu, L. Sun, M. Liu, X. Qiu, W. Xu, *J. Am. Chem. Soc.* **2022**, *144*, 5023–5028.
[17] a) T. Mitsui, M. K. Rose, E. Fomin, D. F. Ogletree, M. Salmeron, *Phys. Rev. Lett.* **2005**, *94*, 036101; b) C. Bertram, W. Fang, P. Pedevilla, A. Michaelides, K. Morgenstern, *Nano Lett.* **2019**, *19*, 3049–3056.
[18] a) C. Zaum, K. Morgenstern, *Phys. Rev. Lett.* **2018**, *121*, 185901; b) W. Fang, K. M. Meyer-auf-der-Heide, C. Zaum, K. Michaelides, K. Morgenstern, *Nano Lett.* **2022**, *22*, 340–346.
[19] a) J. Weckesser, J. V. Barth, K. Kern, *J. Chem. Phys.* **1999**, *110*, 5351–5354; b) R. Otero, F. Hümmelink, F. Sato, S. B. Legoas, P. Thostrup, E. Lægsgaard, I. Stensgaard, D. S. Galvão, F. Besenbacher, *Nat. Mater.* **2004**, *3*, 779–782; c) B. A. J. Lechner, H. Hedgeland, J. Ellis, W. Allison, M. Sacchi, S. J. Jenkins, B. J. Hinch, *Angew. Chem. Int. Ed.* **2013**, *52*, 5085–5088; *Angew. Chem.* **2013**, *125*, 5189–5192; d) G. Antczak, W. Kamiński, A. Sabik, C. Zaum, K. Morgenstern, *J. Am. Chem. Soc.* **2015**, *137*, 14920–14929; e) P. Rotter, B. A. J. Lechner, A. Morherr, D. M. Chisnall, D. J. Ward, A. P. Jardine, J. Ellis, W. Allison, B. Eckhardt, G. Witte, *Nat. Mater.* **2016**, *15*, 397–401; f) D. Civita, M. Kolmer, G. J. Simpson, A. P. Li, S. Hecht, L. Grill, *Science* **2020**, *370*, 957–960.
[20] M. Eichberger, M. Marschall, J. Reichert, A. Weber-Bargioni, W. Auwärter, R. L. C. Wang, H. J. Kreuzer, Y. Pennec, A. Schiffrin, J. V. Barth, *Nano Lett.* **2008**, *8*, 4608–4613.
[21] M. Müller, J. Henzl, K. Morgenstern, *Chem. Phys. Lett.* **2020**, *738*, 136906.
[22] F. Silly, *RSC Adv.* **2020**, *10*, 5742–5746.
[23] a) M. Böhringer, K. Morgenstern, W.-D. Schneider, R. Berndt, *Surf. Sci.* **2000**, *457*, 37–50.
[24] M. Schunack, T. R. Linderoth, F. Rosei, E. Lægsgaard, I. Stensgaard, F. Besenbacher, *Phys. Rev. Lett.* **2002**, *88*, 156102.
[25] D. Kühne, F. Klappenberger, W. Krenner, S. Klyatskaya, M. Ruben, J. V. Barth, *Proc. Natl. Acad. Sci. USA* **2010**, *107*, 21332–21336.

Manuscript received: August 18, 2022
Accepted manuscript online: September 2, 2022
Version of record online: September 29, 2022